Merging Heterogeneous Graphitic Carbon Nitride Photocatalysis with Cobaloxime Catalysis in Uphill Dehydrogenative Synthesis of Anilines

Sonia Zoltowska,‡,[a] Stefano Mazzanti,‡,[a] Sara Stolfi,[b,c] Jingsan Xu,[d] Matej Huš,[e,f,g], Ana Oberlintner[e], Matic Pavlin[e], Paolo Ghigna,[b] Blaž Likozar,[e] Piero Torelli,[c] Luca Braglia,[c] Davide Ravelli,[b] Maurizio Fagnoni,[b] Iker Agirrezabal-Telleria,[h] Markus Antonietti,[a] Paolo Giusto,[a] Oleksandr Savateev*,[i]

‡ these authors contribute equally

[a] Department of Colloid Chemistry, Max Planck Institute of Colloids and Interfaces, Am Mühlenberg 1, D-14476 Potsdam, Germany

[b] Department of Chemistry, University of Pavia, viale Taramelli 12, Pavia 27100, Italy

[c] TASC Laboratory CNR–IOM, Istituto Officina dei Materiali, Trieste 34149, Italy

[d] Queensland University of Technology, Australia

[e] National Institute of Chemistry, Department of Catalysis and Chemical Reaction Engineering, Hajdrihova 19, 1000 Ljubljana, Slovenia

[f] Association for Technical Culture of Slovenia (ZOTKS), Zaloška 65, 1000 Ljubljana, Slovenia

[g] Institute for the Protection of Cultural Heritage of Slovenia (ZVKDS), Poljanska 40, 1000 Ljubljana, Slovenia

[h] Department of Chemical and Environmental Engineering of the Bilbao Engineering School, University of Basque Country (UPV/EHU), Plaza Torres Quevedo 1, Bilbao 48013, Spain

[i] Department of Chemistry, The Chinese University of Hong Kong, Sha Tin, New Territories, Hong Kong, China

Abstract: Synthesis of substituted anilines upon nucleophilic addition of secondary amines to cyclohexanone derivatives followed by aromatization of the enamine by employing a combination of Ir-polypyridine complex as a photoredox catalyst and cobaloxime as H_2-evolution catalyst was developed recently by Leonori et al. In this work, we replace homogeneous photoredox catalyst by heterogeneous mesoporous graphitic carbon nitride (mpg-CN) that is free of rare elements. Substituted aromatic amine and H_2 are formed simultaneously. Combination of X-Ray spectroscopies revealed charge transfer from cobaloxime to mpg-CN in the dark. Illumination of the catalytic system with visible light induces electron transfer from mpg-CN to cobaloxime and formation of persistent Co(II) species. The results of DFT modelling suggest that the studied reaction is strongly endothermic and endergonic. Thus, energy of photons is stored in the reaction products – H_2 and the aromatic amine.

Introduction

The second law of thermodynamics allows predicting if a certain chemical reaction is spontaneous or non-spontaneous in the given conditions. In practice, it requires computing and/or measuring change of enthalpy (ΔH), entropy (ΔS) and computation of Gibbs free energy (ΔG) of a chemical system that undergoes a chemical reaction. Many chemical reactions are characterized by positive change in ΔG, making the reaction thermodynamically non-spontaneous (**Fig. 1**, path A). There are several approaches that enable such intrinsically endergonic reactions. For instance, a commonly exploited approach in chemistry laboratories involves coupling of a desired intrinsically endergonic reaction ($\Delta G_i > 0$) with another highly exergonic one ($\Delta G_j < 0$) so that $\Delta G_j < -\Delta G_i$ – overall Gibbs free energy change of the sum of these two reactions is negative (**Fig. 1**, path B). In practice, compounds with weakly negative or even positive enthalpy of formation are added into the reaction mixture. The energy that is released upon their conversion into thermodynamically more stable compounds is employed to drive the desired intrinsically uphill reaction. This approach naturally generates chemical waste and decreases atom efficiency. More innovative, but at the same time more challenging approach, is to lift the Gibbs free energy of the reactants, to afford $\Delta G < 0$ (**Fig. 1**, path C).[1,2] This approach is realized in electrolysis (or electrocatalysis), photochemistry (or photocatalysis) and plasma catalysis.[3] Typically, charged radical species generated upon oxidation, reduction or ionization of substrates and electronically excited state of compounds obtained upon photon absorption are highly reactive. Therefore, in general, they undergo transformations into more stable species spontaneously.

One of the most studied intrinsically endergonic reactions is water dissociation into H_2 and O_2. This reaction does not occur spontaneously under the standard conditions, ΔG^{298} of the reaction $2H_2O \longrightarrow 2H_2 + O_2$ is +113 kcal mol^{-1}. However, the reaction proceeds when energy is supplied by photons or electromotive force. When this energy in the form of electricity for electrolysis or light for photocatalysis is derived from renewable sources, the generated H_2 is considered *green*. While the by-product of water splitting, O_2, is less valuable, electrocatalytic or photocatalytic water splitting can afford oxygen of high purity to complement the existing air separation technology. An alternative approach considers generation of H_2 from hydrogen-rich organic compounds, coupled with their conversion into value-added products. The examples of products synthesized via this approach are represented by chemical commodities, such as acetaldehyde[4,5,6,7,8] or 2,3-butandiol[9,10,11,6] that are obtained upon dehydrogenation of ethanol, ethylene glycol – from methanol,[12,13,14,15] and other organic compounds.[16,17,18] It is worth to mention that the demand for such fine organic compounds is significantly lower compared to the above mentioned industrial commodities. Given that H_2 and organic compounds are generated in stoichiometric, ~1:1, ratio, various oxidant-free cross-dehydrogenative coupling[19] and cross-coupling hydrogen evolution reactions[20] cannot, in principle, fulfil all the demand in H_2. Nevertheless, these strategies to construct more complex organic compounds are more atom efficient – *i*) prefunctionalization of the organic substrates is avoided, *ii*) the "by-products" are H_2, H_2O, CO_2 and/or other small molecules.[21,22,23,15, 24] More promising is generation H_2 from biomass, such as lignin, cellulose[25] or pollutants.[26] However, the yield rate of H_2 is significantly lower compared to model small organic sacrificial molecules – glucose, and other sugars.[27] It is also of fundamental interest to expand the scope of dehydrogenation reactions and identify which of them are intrinsically endergonic, but are enabled by means of photochemistry and photocatalysis. In this case the energy of photons is stored in the organic products, while the reaction is regarded as artificial photosynthesis.[28]

Recently, Leonori et al. developed an elegant approach to synthesize substituted anilines from aliphatic ketones and amines employing a combination of Ir-polypyridine photoredox catalyst and $Co(dmgH)_2(Me_2NPy)Cl$ (**Fig. 1B**).[29] The method shows several advantages – *i*) there are many precursors available commercially, and *ii*) in addition to substituted anilines two H_2 and one H_2O equivalents are generated as the by-products. On the other hand, *i*) it relies on Ir-based photoredox catalyst – this transition metal is rare and expensive, and *ii*) endo-/exoergicity of the reaction was not assessed. These aspects prompted us to gain the missing pieces of information and to develop a complimentary method that does not require Ir complexes as photocatalyst.

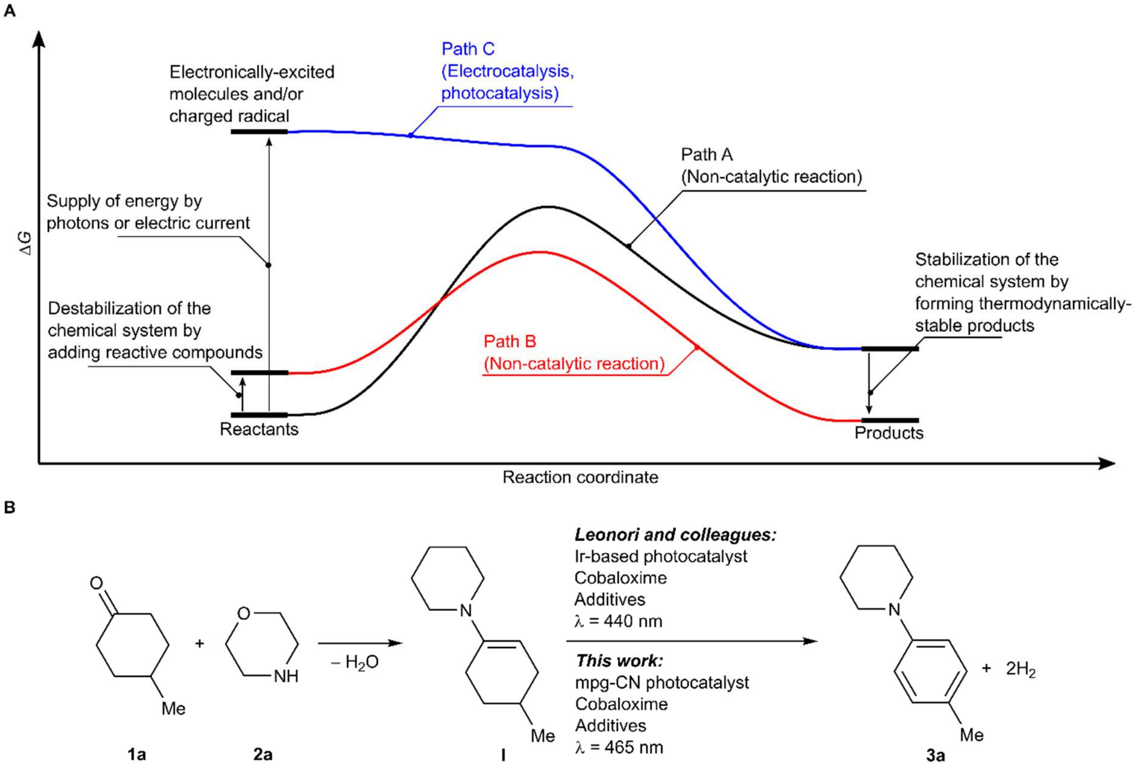

Fig. 1. **A**: Path A denotes schematically a reaction profile of a certain endergonic reaction and synthesis of a target compound. Path B denotes synthesis of the target compound when it is coupled with another exergonic reaction. Path C denotes photochemical, electrochemical approaches or plasma catalysis that involve formation of reactive intermediates – radical ions and electronically-excited states. **B**: Synthesis of anilines from aliphatic ketones and amines that is accompanied by H_2 evolution reported by Leonori and colleagues.

Herein, we present a method of anilines synthesis from aliphatic ketones and amines that is enabled by mesoporous graphitic carbon nitride (mpg-CN) as the heterogeneous photocatalyst coupled with commercial $Co(dmgH)_2PyCl$ as H_2-evolution catalyst.

Results and Discussion

First, the thermodynamics of the involved reactions was calculated to ascertain their feasibility and spontaneity. The condensation of **1a** and **2a** into **I** is thermoneutral for practical purposes (ΔH^{298} = +1.56 kcal mol^{-1}) and slightly endergonic (ΔG^{298} = +2.88 kcal mol^{-1}) in standard conditions (**Fig. 1B**). The equilibrium constant can be shifted by changing the temperature and the equilibrium composition can be influenced by changing the fraction of reactants and products, including water. Thus, the step is not a thermodynamic bottleneck. A subsequent conversion of **I** into **3a**, where two molecules of H_2 are also formed, is strongly endothermic (ΔH^{298} = +39.24 kcal mol^{-1}). The formation of two hydrogen molecules increases the entropy of the system, offsetting some increase in the Gibbs free energy (ΔG^{298} = +7.82 kcal mol^{-1}). Thus, a fraction of photon energy is stored in the products.

We studied synthesis of **3a** from 4-methylcyclohexanone **1a** as a saturated aryl surrogate and morpholine **2a**. Their interaction with the formation of **I** occurs spontaneously, in agreement with the results of thermodynamic calculations. Following the procedure proposed by Leonori and colleagues[29] we tested a catalytic system based on mpg-CN and $Co(dmgH)_2PyCl$ complex (**Fig. 1B**). In our reaction system, mpg-CN serves as the photocatalyst, which electronically excited state is quenched reductively by **I**, while $Co(dmgH)_2PyCl$ functions as the dehydrogenation catalyst. The results of the reaction conditions optimization are summarized in Table 1.

Table 1. Screening of the reaction conditions of aniline synthesis.

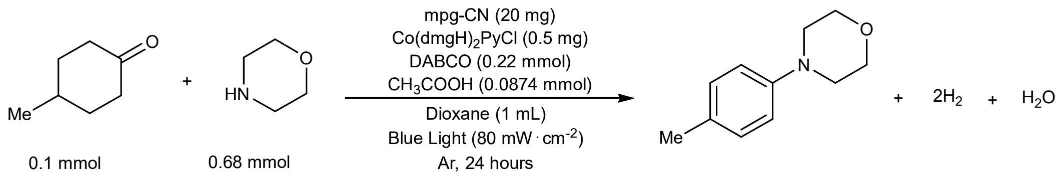

1a **2a** **3a**

Entry	Deviations from standard conditions	Yield (%)[a]
1	None[b]	49
2	Na-PHI	9
3	Without mpg-CN	n.d.
4	Without $Co(dmgH)_2PyCl$	n.d.
5	In the dark	n.d.
6	mpg-CN; Purple LED[c]	16
7	mpg-CN; UV LED[d]	27
8	mpg-CN; $Co(dmgH)_2PyCl$ (0.0024 mmol)	48
9	mpg-CN; $Co(dmgH)_2PyCl$ (0.0048 mmol)	50
10	mpg-CN (30 mg)	44
11	mpg-CN (10 mg)	46
12	mpg-CN (5 mg)	32
13	mpg-CN; air	28
14	mpg-CN; without DABCO	10
15	mpg-CN; without AcOH	30

[a] GC yield

[b] Reaction conditions: ketone (0.1 mmol, 0.125 mL), morpholine (0.68 mmol, 0.59 mL), mpg-CN 20 mg, Co(dmgH)$_2$PyCl (0.0012 mmol, 0.5 mg), DABCO (0.22 mmol, 25 mg), glacial AcOH (0.0874 mmol, 0.005 mL), dioxane (1 mL), blue LEDs (λ_{max} = 460 nm, 80 mW cm^{-2}), 25 °C, 24 h, n.d. – not detected.

[c] λ_{max} = 400 nm, 60 mW cm^{-2}

[d] λ_{max} = 365 nm, 60 mW cm^{-2}

The yield of aniline **3a** synthesized under the optimal reaction conditions reaches 49%. The screening of the reaction conditions indicates the crucial role of DABCO as a proton shuttle, which might be involved in the photocatalytic cycle as well as cobaloxime turnover step. Furthermore, the presence of acid and the absence of oxygen are necessary to obtain a satisfactory product yield. No product is obtained without the addition of mpg-CN or Co(dmgH)$_2$PyCl, highlighting their importance for the synthesis of **3a**. Similarly, no product is observed when the reaction is performed in the dark, demonstrating the photochemical nature of the process. Notably, increasing the amount of Co(dmgH)$_2$PyCl does not significantly increase the yield of **3a**, underscoring the synergistic action of mpg-CN and Co(dmgH)$_2$PyCl.

Stability of a catalytic system is crucial to evaluate its lifespan, resistance to deactivation, and overall durability, which are essential for maintaining consistent performance. Therefore, the reusability tests have been performed with and without the refilling of Co(dmgH)$_2$PyCl, details can be found in Supplementary note 1. The results indicate that mpg-CN may be reused, but deactivation of Co(dmgH)$_2$PyCl occurs. Therefore, addition of a fresh portion of Co(dmgH)$_2$PyCl is required. Generation of H_2 and aniline simultaneously was confirmed in the experiment conducted on 7 mmol scale of 4-methylcyclohexanone resulting in formation of aniline with 35% yield (**Fig. S2**). A combination of mpg-CN and Co(dmgH)$_2$PyCl mediates the synthesis of anilines by coupling various aliphatic ketones with amines (**Fig. S3**, **Table S1**).

To understand the reaction mechanism, it is essential to elucidate the roles of mpg-CN and Co(dmgH)$_2$PyCl. Consequently, a comprehensive characterization of the physicochemical properties of these materials was conducted. Detailed results of these characterizations are provided in Supplementary note 3.

X-Ray absorption spectroscopy (XAS) and X-Ray photoelectron spectroscopy (XPS) were employed to get insights into the reaction mechanism and the electronic properties of the bare mpg-CN and the composite Co(dmgH)$_2$PyCl (2.4 wt. %)/mpg-CN, which was prepared by concentrating a mixture of mpg-CN and Co(dmgH)$_2$PyCl in vacuum. The mass fraction of cobaloxime in Co(dmgH)$_2$PyCl/mpg-CN is equal to that in entry 1 of **Table 1**. As shown by N 1s XPS spectrum, the introduction of Co(dmgH)$_2$PyCl results in the shift of the peaks that are assigned to C−N=C and N-C$_3$ moieties in mpg-CN by ~0.3 eV and C-NH$_X$ species by ~0.2 eV to lower binding energies. Such shift suggests charge transfer from Co(dmgH)$_2$PyCl to N-atoms of mpg-CN. Similar direction of charge transfer from cobaloxime to mpg-CN and the magnitude of the peaks shift, ~0.2-0.3 eV, is observed in the O 1s XPS spectrum (see **Fig. S8**). In C 1s spectrum, the magnitude of the peaks shift is lower, ~0.2 eV, which might be explained by more preferable coordination of Co by N and O-atoms compared to C. Although XPS provides detailed information on the surface binding schemes and the electron density changes at the materials surface chemical features, XANES provides complementary information especially for the study of the oxidation state changes at the Co L-edge, before and after the reaction.

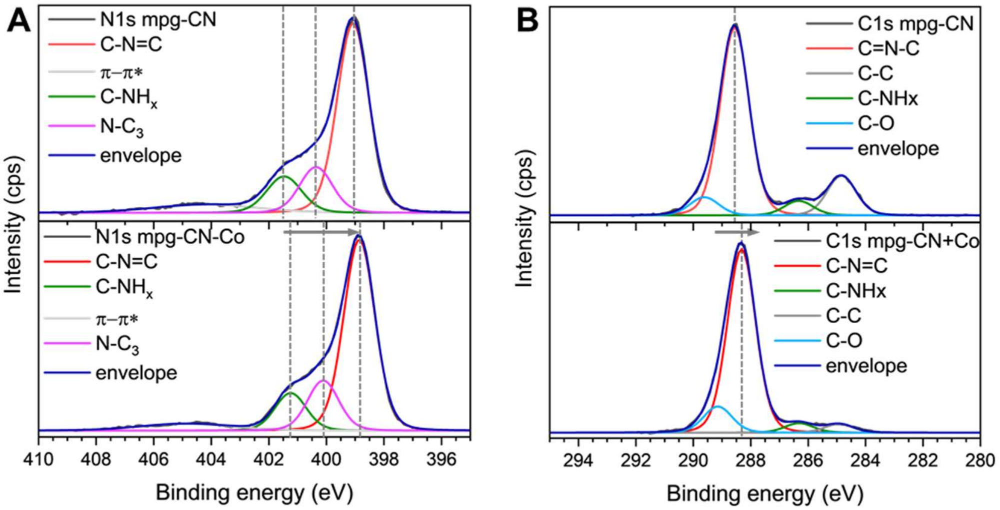

Fig. 2. XPS analysis of mpg-CN and Co(dmgH)$_2$PyCl/mpg-CN: N 1s (A), C 1s (B).

The XANES spectrum Co(dmgH)$_2$PyCl/mpg-CN in dark reveals that Co is in the oxidation state +3 (**Fig. 3A**). Upon illumination of the sample with visible light (405 nm) we record a major change in the Co peak shape with the arising of two peaks located at 776.4 and 775.3 eV in the L$_3$ edge spectrum pointing to a reduction of Co(III) to Co(II). At the N K-edge, complementary changes are observed: the spectrum shifts towards higher energy values upon illumination, pointing to a charge transfer from the mpg-CN to the cobalt. Thus, the edge energy position in the XANES spectrum is a measure of the ionization potential of the corresponding N core level (1s for the K-edge). This is shielded by all the other (valence) electrons, and therefore a shift of the edge position towards higher energy indicates less shield and therefore, in chemical terms, an oxidation. The described changes in N K-edge and Co L-edge spectra are at least partially reversible: cessation of light irradiation leads to slow partial recovery of Co(III) and charge transfer back to mpg-CN. However, it is worth mentioning that some changes, after prolonged irradiation, are not reversed (in the time of the experiment). For example, at the N K-edge, there is a broadening of both the main peak at ~402.5 eV and of the peak at ~405.5 eV, that is not reversed[30]. In summary, the XAS results are consistent with a scenario where the UV photons create electron-hole couples, where the hole is localized on mpg-CN, while the electron is localized on the Co of the cobaloxime. Co(II) species are long-lived and may be the resting state of cobaloxime. X-Ray absorption spectroscopy studies of Co-polypyridyl complex and Co(dmgBF$_2$)$_2$ identified Co(I) species, which are formed transiently upon Co-complex excitation in the presence of sacrificial electron donors – ascorbic acid or triethanolamine.[31,32] These conditions, however, are different from that employed in our current study – Co(dmgH)$_2$PyCl/mpg-CN was investigated in solid state in vacuum without adding any sacrificial agents.

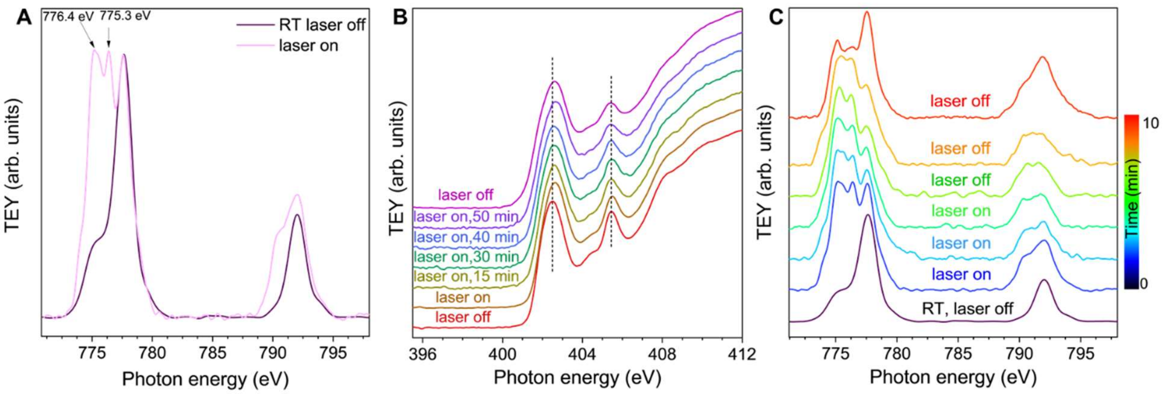

Fig. 3. Co $L_{2,3}$-edge spectra of and Co(dmgH)$_2$PyCl/mpg-CN without (purple line) and with illumination (pink line) (A), N K-edge spectra without (red line) (B) and Co $L_{2,3}$-edge spectra (C) with illumination (different colors), and with the laser switched off after illumination (red line).

Theoretical calculations were conducted to elucidate the reaction mechanism in more detail. First, **I** is adsorbed into pores on the (**ac**) surface of mpg-CN with an adsorption interaction of 1.18 eV (27.1 kcal mol^{-1}). Upon excitation to *mpg-CN, four H$^+$/e$^-$ pairs are transferred, forming 4 equivalents of mpg-CN(H$^+$/e$^-$) as **I** is converted through **II**, **III** and **IV** to **3a** (see **Fig. 4** for the energy profile). The overall energy change during those steps is −2.4 kcal mol^{-1}, i.e., energy difference between "**I** + 4 mpg-CN" and "**3a** + 4 mpg-CN(H$^+$/e$^-$)".

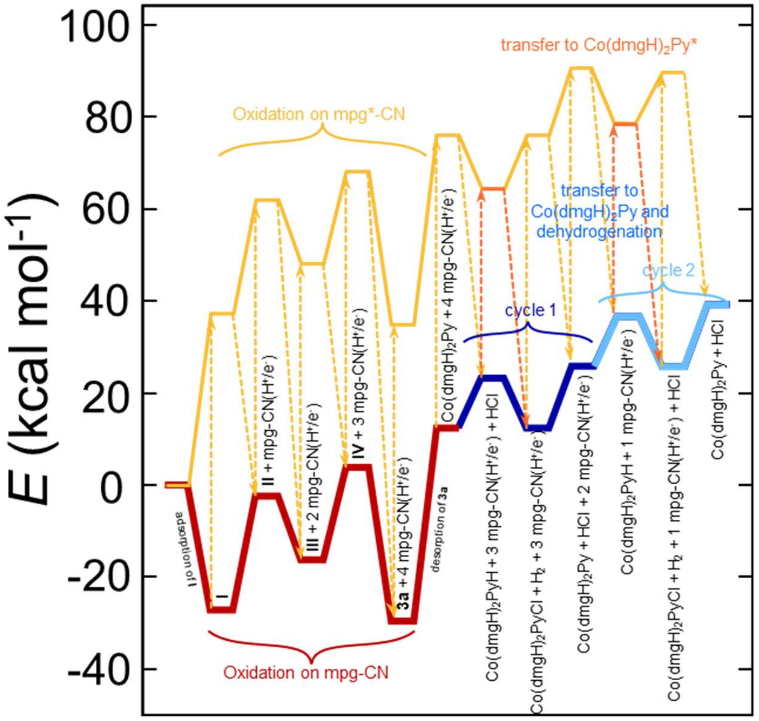

Fig. 4. The energy profile for oxidation of **I** and dehydrogenation of mpg-CN(H$^+$/e$^-$) by Co(dmgH)$_2$PyCl to produce H_2. Vertical lines represent excitation of a chemical system upon photon absorption.

TDDFT determined energy of the mpg-CN excited state is 62 kcal mol^{-1}, and of the Co species is +43 kcal mol^{-1}.

As discussed earlier, the uncatalyzed reaction (thermodynamic limit) has an energy change of +39.2 kcal mol^{-1}. This difference, which accounts for the superior performance of mpg-CN, is explained by a strong adsorption of **3a** (−41.9 kcal mol^{-1}, i.e., energy difference between **3a** adsorbed on mpg-CN and desorbed **3a** + mpg-CN) and the propensity of mpg-CN to attract hydrogen. Relative to $H^+ + e^-$ (which is equilibrium with ½ H_2 at SHE conditions), mpg-CN(H^+/e^-) with H^+ at the most favourable site has a −0.29 eV (−6.7 kcal mol^{-1}) lower energy than mpg-CN, indicating a facilitated transfer (see **Fig. 5** for the comparison). The preferential storage of H^+ in a "triangular pocket" of the **(ac)** surface of mpg-CN agree with the results of modelling obtained earlier.[33]

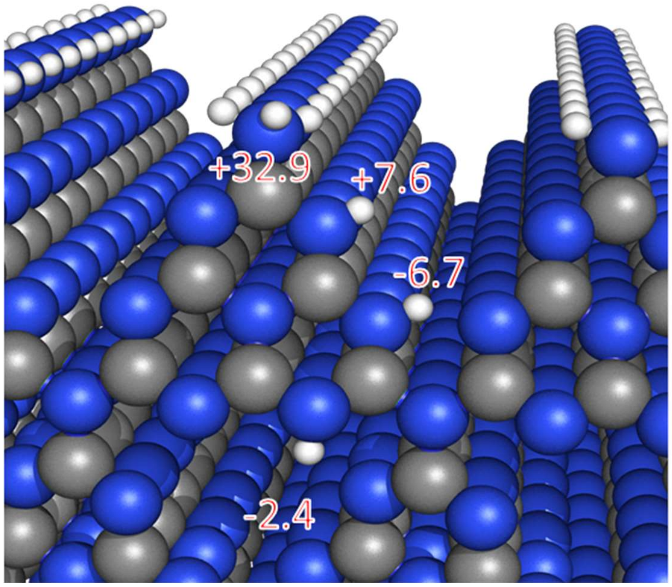

Fig. 5. Possible sites for binding H* on the **(ac)** plane of mpg-CN. Values represent adsorption energy (in kcal mol^{-1}) relative to ½ H_2. Negative values indicate favorable adsorption.

Subsequently, dehydrogenation occurs as mpg-CN(H^+/e^-) transfers hydrogen atoms to the Co^{II} complex ($Co^{II}(dmgH)_2Py$). Note that XAS measurements revealed Co(II) being persistent species. In the first step, a single hydrogen atom is transferred, forming $Co^{III}(dmgH)_2PyH$. In the next step, $Co^{III}(dmgH)_2PyH$ reacts with H^+Cl^-, being converted to $Co^{III}(dmgH)_2PyCl$ and releasing H_2. The cobalt complex is recovered upon a reaction with the second equivalent of mpg-CN(H^+/e^-), forming mpg-CN, HCl and $Co^{II}(dmgH)_2Py$. The whole reaction pathway is shown in **Fig. 6**.

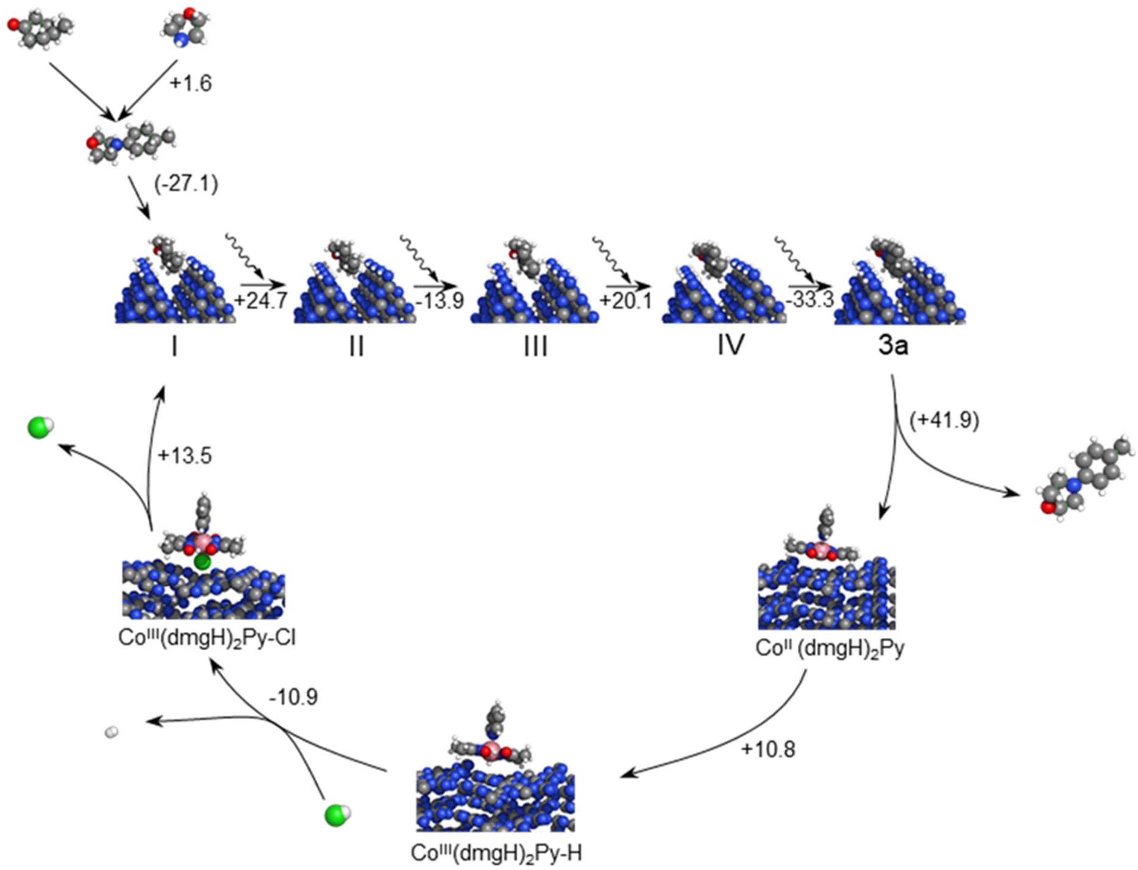

Fig. 6. A complete reaction mechanism along with the energy differences for each reaction step (in kcal mol^{-1}). Adsorption/desorption energies are shown in parentheses. The steps involving the Co-complex transfer 2 H^+/e^- and must occur twice in a cycle (see **Fig. 8**).

Lastly, we studied the effect of different Co-complexes. Co^{II}(dmgH)$_2$Py was modelled to get insights into the results of XAS measurements. In the unbound Co^{II}(dmgH)$_2$Py, Co is formally in the oxidation state of +2. The natural bond orbital (NBO6) analysis shows that Co has a net charge of 0.99 e_0. Upon a H^+/e^- transfer, the metal centre in Co(dmgH)$_2$PyH is partially reduced to 0.63 e_0, while the newly transferred H retains its electron (charge 0.02 e_0). Upon full oxidation, the charge on Co in the ensuing Co^{III}(dmgH)$_2$PyCl is 0.86 e_0. In **Fig. 7**, HOMO and LUMO are shown. This reveals two important considerations. First, formal oxidation states are rough approximations at best, which only qualitatively follow the calculated values, while the difference in the calculated charges during the reaction is much less extreme. Secondly, in Co^{III}(dmgH)$_2$PyCl the Co atom is (ever so slightly) *less* oxidised compared to Co^{II}(dmgH)$_2$Py. This difference is, however, even smaller when in contact with mpg-CN (1.02 vs 1.09 e_0), where some charge transfer is also observed (*vide infra*).

Co^{II}(dmgH)$_2$Py and Co^{III}(dmgH)$_2$PyCl must approach the catalyst for an efficient hydrogen transfer. Simulations show that the cobaloxime can only approach mpg-CN from the side along the (**ab**) facet. Their interaction energy is similar, 25.3 and 24.1 kcal mol^{-1}. As shown by XAS and XPS, there is considerable charge transfer to mpg-CN. The Bader charge of the unperturbed surface N atoms in mpg-CN is -1.1 e_0. Co^{II}(dmgH)$_2$Py is positioned with Co above one N atom, which has a Bader charge of

-2.0 e_0. On the other hand, $Co^{III}(dmgH)_2PyCl$ is roughly between two surface N atoms, which have Bader charges of -1.81 e_0 and -1.67 e_0, indicating a cumulatively larger charge transfer. This is also graphically shown in **Fig. 7**.

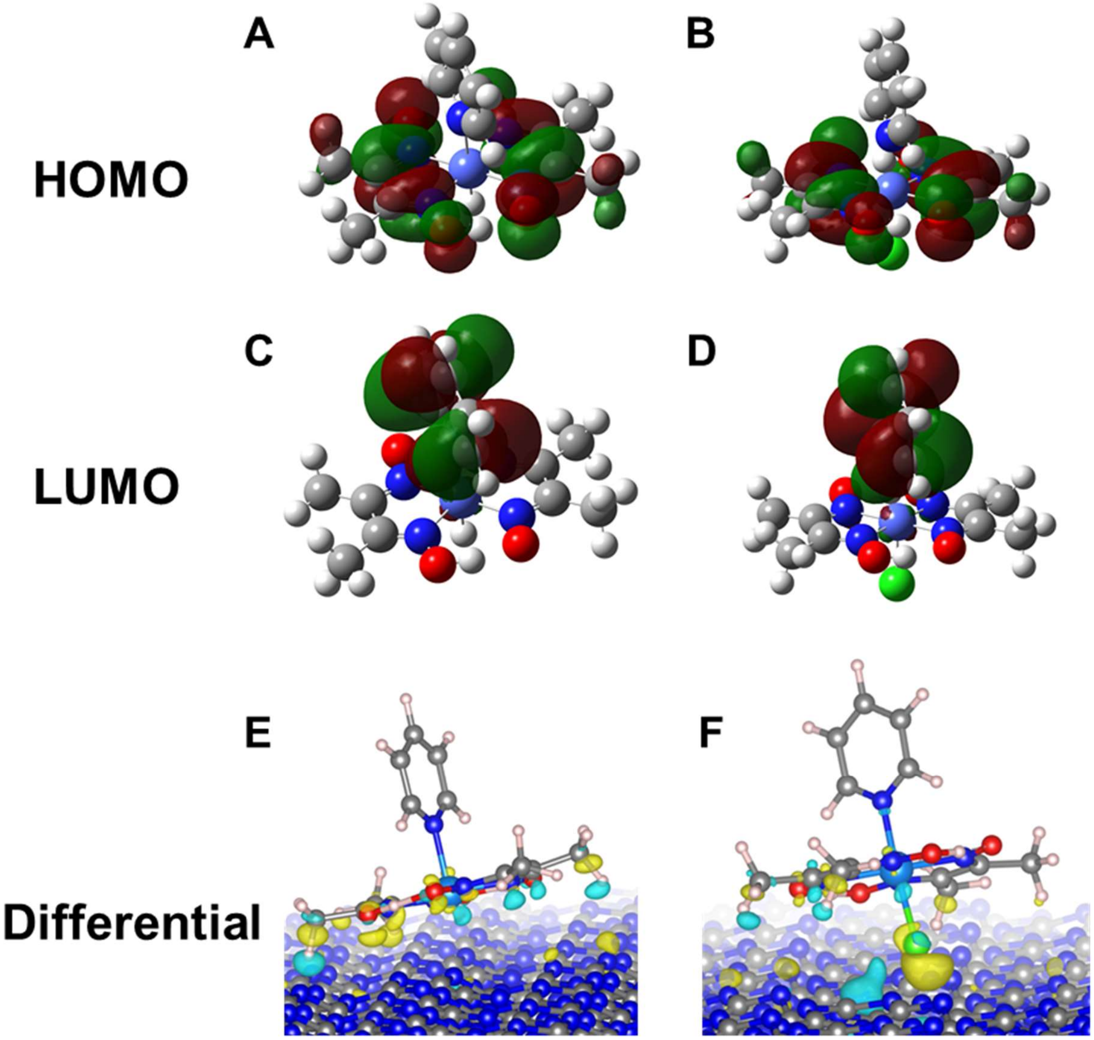

Fig. 7. Depiction of HOMO (top), LUMO (middle) orbitals and differential charge density upon adsorption to mpg-CN (bottom) of $Co^{II}(dmgH)_2PyH$ (left) and $Co^{II}(dmgH)_2PyCl$ (right).

Leonori and colleagues concluded involvement of two photons for each molecule of aniline formed.[29] The results of modelling revealed energy barriers greater than ~30 kcal mol^{-1} (oxidation on mpg-CN) and greater than ~10-20 kcal mol^{-1} (cobaloxime cycle). Given that all the experiments were conducted at ~25-35 °C, it is unlikely that the ambient environment can provide sufficient energy to overcome the energy barriers by heat only. Therefore, involvement of more than two photons per each molecule of aniline formed is deemed to be reasonable, which is reflected in **Fig. 8**.

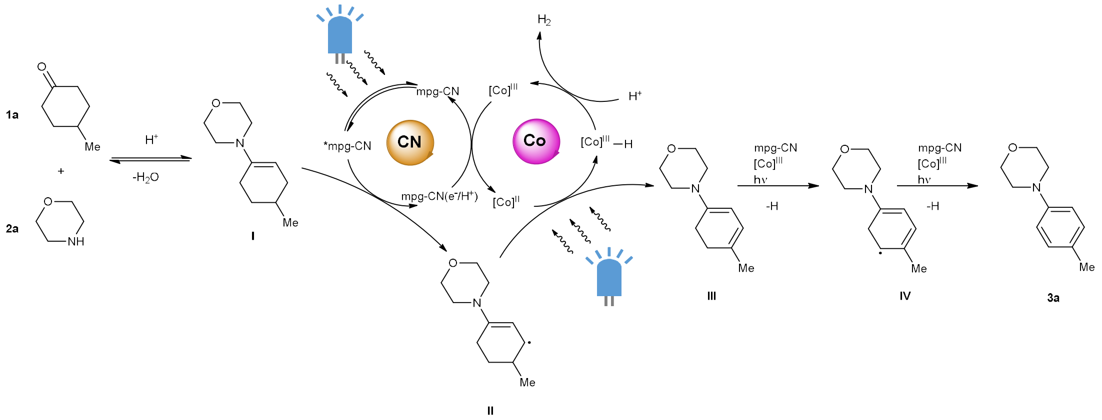

Fig. 8. A proposed photocatalytic mechanism of **3a** synthesis by employing a combination of $Co(dmgH)_2PyCl$ and mpg-CN.

Conclusions

The photocatalytic synthesis of substituted anilines from carbonyl compounds and amines, a reaction of critical importance in synthetic chemistry, has traditionally relied on molecular catalysts based on rare-earth elements, which poses sustainability challenges. This study demonstrates that merging the mesoporous graphitic carbon nitride (mpg-CN) with cobaloxime can serve as an effective alternative to molecular catalysts in the synthesis of substituted anilines. Specifically, a combination of mpg-CN and a cobaloxime facilitates aromatization of enamine that is accompanied by evolution of hydrogen. This method efficiently couples aliphatic ketones with amines to produce substituted anilines and hydrogen in a heterogeneous manner. Mechanistic studies, supported by X-ray spectroscopy and DFT calculations, reveal charge transfer from cobaloxime to mpg-CN in the dark and light-induced electron transfer from mpg-CN to cobaloxime, leading to the formation of persistent Co(II) species. This process effectively stores photon energy in the reaction products, making the energetically uphill reaction feasible. Furthermore, detailed catalyst characterization under reaction conditions confirmed the formation of a heterojunction, underscoring the efficacy of the proposed catalytic system for the synthesis of anilines using various ketones. This method not only demonstrates the potential for more sustainable and efficient production of anilines but also highlights the importance of integrating heterogeneous photocatalysts with molecular catalysts for advanced organic transformations.

Experimental section

Reagents were purchased at the highest commercial quality and used without further purification.

Synthetic procedures

Catalyst preparation: mpg-CN was prepared using the following steps: cyanamide (30 g) was mixed with an aqueous colloidal suspension of silica (75 g, LUDOX HS-40, 40 wt%) until a clear solution was obtained. The mixture was then subjected to slow evaporation using a rotary evaporator until it formed a transparent amorphous solid. Next, the flask containing the solid was promptly placed into a water bath preheated to 80 °C and connected to a gas trap. As the solid heated, it turned white, and the evolution of ammonia was observed. The white solid was subsequently transferred to a crucible and heated in an oven at 550 °C for 4 hours, followed by additional calcination at the same temperature for another 4 hours under a flow of nitrogen. After cooling, the contents of the crucible were transferred to a polypropylene bottle, into which NH_4HF_2 (120 g) and water (500 mL) were added. The mixture was stirred for 24 hours. Following filtration, the solid was washed multiple times with water and ethanol before being dried overnight in a vacuum oven. The final yield was 15.8 g.

General procedure dehydrogenative synthesis of anilines: A 5-mL vial was fitted with a magnetic stirrer and filled with mpg-CN (20 mg), chloro(pyridine)bis(dimethylglyoximato)cobalt(III) (0.5 mg, 0.0012 mmol), and DABCO (25 mg, 0.22 mmol), all mixed thoroughly. Subsequently, 1,4-dioxane (1 mL), 4-methylocyclohexan-1-one (0.0125 mL, 0.1 mmol), morpholine (0.059 mL, 0.68 mmol), and CH_3COOH (0.005 mL, 0.0874 mmol) were added to the mixture. The vials were sealed with screw caps equipped with a PTFE liner and degassed with Ar using a double needle technique. The reaction mixture was then irradiated for 24 hours inside a blue photoreactor (λ_{EM} = 465 nm, E_{EM} = 80 mW cm^{-2}). After the reaction, the catalyst was separated by centrifugation, and the solution was transferred back into the vial for analysis by GC-MS.

General procedure for scale-up experiment: In a three-neck reactor equipped with a magnetic stirring bar, mpg-CN (1.4 g), chloro(pyridine)bis(dimethylglyoximato)cobalt(III) (35 mg, 0.084 mmol), and DABCO (1.75 g, 15.7 mmol) were placed and thoroughly mixed. Subsequently, 1,4-dioxane (70 mL), 4-methylocyclohexan-1-one (0.875 mL, 7 mmol), morpholine (4.13 mL, 47.6 mmol), and CH_3COOH (0.35 mL, 6.125 mmol) were added to the mixture. The reactor was then degassed with Ar, and the temperature sensor was immersed while the gas collector was connected to the reactor neck. The reaction mixture was irradiated for 24 hours inside a blue photoreactor. After the 24-hour reaction period, the reaction mixture (1 mL) was extracted, the catalyst was separated by centrifugation, and the solution was analyzed by GC-MS. The reaction was considered complete when all starting materials were consumed. The catalyst was further separated from the reaction mixture by centrifugation. Subsequent steps involved the isolation of the reaction product. Firstly, the dioxane was removed using a rotary evaporator. Then, dichloromethane was used to dissolve the remaining liquid. Next, the solution was washed successively with sodium bicarbonate, water, and brine. Finally, the solvent was removed using a rotary evaporator. Purification of the crude liquid was carried out by hand column chromatography using ethyl acetate/hexane as eluents on silica gel.

General procedure for catalyst stability tests: The reaction was performed in a 5-mL vial as previously described. In the first experiment, the recovered catalyst was washed with ethanol, dried, and then reused for another reaction. After 24 hours of irradiation, the catalyst was recovered by centrifugation, washed with ethanol, and dried at 60°C in a vacuum oven. After each catalytic run, the reaction mixture was collected and analyzed by GC-MS.

In the second experiment, the chloro(pyridine)bis(dimethylglyoximato)cobalt(III) was replenished. After the first catalytic run, the catalyst was recovered, washed with ethanol and dried at 60°C. For the second reaction cycle, the recovered catalyst was combined with an additional chloro(pyridine)bis(dimethylglyoximato)cobalt(III) (0.5 mg, 0.0012 mmol) and the standard reaction mixture. After 24 hours of irradiation, the catalyst was again recovered, washed and dried. This procedure was repeated for a third cycle with the addition of a fresh portion of the cobaloxime (0.5 mg, 0.0012 mmol). After each catalytic run, the reaction mixture was collected and analyzed by GC-MS.

General procedure for reactions with different ketones in 0.1 mmol scale: A 5-mL vial was fitted with a magnetic stirrer and filled with mpg-CN (20 mg), chloro(pyridine)bis(dimethylglyoximato)cobalt(III) (0.5 mg, 0.0012 mmol), and DABCO (25 mg, 0.22 mmol), all mixed thoroughly. Subsequently, 1,4-dioxane (1 mL), chosen ketone (0.1 mmol), morpholine (0.059 mL, 0.68 mmol), and CH_3COOH (0.005 mL, 0.0875 mmol) were added to the mixture. The vials were sealed with screw caps equipped with a PTFE liner and degassed with Ar using a double needle technique. The reaction mixture was then irradiated for 24 hours inside a blue photoreactor (λ_{EM} = 465 nm, E_{EM} = 80 mW cm^{-2}). After the reaction, the catalyst was separated by centrifugation, and the solution was transferred back into the vial for analysis by GC-MS.

General procedure for reactions with different ketones in 5 mmol scale: In a three-neck reactor with a magnetic stirring bar, mpg-CN (1 g), chloro(pyridine)bis(dimethylglyoximato)cobalt(III) (25 mg, 0.06 mmol), and DABCO (1.25 g, 11 mmol), was combine and mixed. Then, 1,4-dioxane (50 mL), along with 4-metoxycyclohexan-1-one (A) or 1,4-cyclohexanedione (B) or and 2-cyclohexen-1-one (C) (5 mmol each), morpholine (2.95 mL, 34 mmol), and CH_3COOH (0.250 mL, 4.375 mmol) were added. After degassing the reactor with Ar, the temperature sensor and connected the gas collector were submerged. The reaction mixture underwent 24 hours of irradiation inside a blue photoreactor. After that time, the reaction mixture (1 mL) was extracted, catalyst was separated by the centrifugation, and the solution was analyzed by GC-MS. The reaction was considered finished when all starting materials were used up. We then isolated the catalyst from the reaction mixture by centrifugation. Next steps included removing dioxane with a rotary evaporator, dissolving the remaining liquid in dichloromethane, washing the solution with sodium bicarbonate, water, and brine, and finally removing the solvent with a rotary evaporator. To purify the crude liquid, we conducted hand column chromatography on silica gel using ethyl acetate/hexane as eluents.

Physicochemical characterization of catalyst:

The crystallinity of the materials was determined by powder X-ray diffraction (XRD) using Rigaku SmartLab (Japan, Cu Kα, 0.154 nm). Thermo Scientific Nicolet iD7 (USA) spectrometer was used as a Fourier-transform infrared (FTIR) spectrometer. Physisorption measurements were performed on a Quantachrome Quadrasorb SI (Austria) at 77 K for N_2. The specific surface areas were calculated by applying the Brunauer-Emmett-Teller (BET) model to adsorption isotherms for $0.05 < p/p_0 < 0.3$ using the QuadraWin 5.11 software package. Samples were degassed overnight before the measurements. Scanning Electron Microscopy (SEM) imaging was performed using the Zeiss LEO 1550-Gemini (Germany) system with acceleration voltage of 10 kV. An Oxford Instruments X-MAX (UK) 80 mm^2 detector was used to collect the energy-dispersive X-ray (EDX) data. Fluorescence spectra were recorded on Jasco FP-830 instrument (Japan). The excitation wavelength was set at 375 nm. Optical absorbance spectra of powders were measured on a Shimadzu UV 2600 equipped with an integrating sphere. EPR study was conducted on Bruker EMXnano benchtop X-Band EPR spectrometer (Germany). The following settings have been used for all spectra acquisition unless other is specified: Center Field 3448.05 G, Sweep Width 200 G, Receiver Gain 50 dB, Modulation Amplitude 1.000 G, Number of Scans 10, Microwave Attenuation 20 dB. Sample were placed and flame-sealed in EPR capillaries (IntraMark, volume 50 µL, ID 0.86 mm), inside the EPR tube (ID 3 mm, OD 4 mm, length 250 mm). Photoluminescence maps were recorded by Horiba FluoroMax-4 (Japan), integration time 0.2, and slits apertures 2. Mass spectral data were obtained using Agilent GC 8890 gas chromatograph, equipped with HP-5MS column (inner diameter = 0.25 mm, length = 30 m, and film = 0.25 µm), coupled with Agilent GC/MSD 5977B mass spectrometer (electron ionization). 1H NMR spectra were recorded on Agilent 400 MHz Bruker (Germany).

Computational methods

Thermodynamic calculations were performed at the DFT level using Gaussian 16. The wB97XD functional[34] was chosen on account of its favourable performance for main-group elements and organo-metallics and inclusion of the D2 dispersion interaction by Grimme. Geometrical optimizations were done with the 6-31+G(d,p) basis set and final energies were obtained as single-pass calculations with the 6-311++G(d,p) basis set. In all instances, the SMD variation of the IEFPCM solvent was used with the default settings for dioxane[35]. Vibrational analysis was performed to confirm that no imaginary frequencies were present in stable structures. Vibrational, rotational and translational contributions to the free energy were accounted for. Gibbs free energies were computed at 1 atm and 298.15 K[36]. These calculations were used to study the thermodynamics and equilibria of the reactions involved in the process.

A combined H^+/e^- transfer from the substrate to mpg-CN was modelled with a plane-wave DFT approach, as implemented in VASP 6.3.1, due to the periodic structure of mpg-CN. It was modelled as a perfectly-condensed graphitic carbon nitride[37]. It assumes an undulating structure with a computationally optimized unit cell a = 7.00, b = 12.12, c = 7.00 Å and $C_{24}N_{32}$ composition. Consistent with previous works, a slightly off-set AA structure, where the layers are shifted by 12% and 7% in the cardinal directions, is most stable. The structure is not planar but assume a zigzag-type geometry, consistent with[38]. The active site of mpg-CN is the (ac) edge plane, which was modelled in a 2x2 supercell with hydrogen-terminated dangling nitrogen atoms ($-NH_2$). Along the (ac) edge, mpg forms pores, where **I** (4-(4-methylcyclohexen-1-yl)morpholine) binds to and undergoes a stepwise oxidation as H^++e^- is transferred to *mpg-CN under illumination. The re-oxidation of mpg-CN(H^+/e^-), however, can only occur at the edges (ab), since the ($Co(dmgH)_2PyCl$) complex does not fit into the pores on (ac). A RPBE functional[39] was used with an energy cutoff of 500 eV. A Gaussian smearing of 0.001 eV was used to improve the electronic convergence. Spin-polarised calculations were used where required and the Grimme D3 dispersion correction was turned on[40] . Due to the size of the supercell, a single point (gamma) sampling in the Brillouin zone sufficed. Whenever multiple possibilities existed, all possible adsorption sites were considered, and the lowest-lying energies are reported universally.

Acknowledgements

This project received funding from the European Union's Horizon Europe research and innovation program under grant agreement no. 101046836 (project acronym "CATART"). The publication reflects only the author's views and the European Union is not liable for any use that may be made of the information content therein. Financial support from the Slovenian Research and Innovation Agency (ARIS) through core funding P2-0152, infrastructure funding I0-0039, and project funding HyBReED, N1-0303, J2-4424, and N2-0310. The authors gratefully acknowledge the HPC RIVR consortium and EuroHPC JU providing computing resources of the HPC system Vega at the Institute of Information Science, Maribor, Slovenia.

Supporting Information

References

1. Zhao, Q.-Q.; Rehbein, J.; Reiser, O., Thermoneutral Synthesis of Spiro-1,4-Cyclohexadienes by Visible-Light-Driven Dearomatization of Benzylmalonates. *Green Chemistry* **2022,** *24*, 2772-2776.
2. Singh, K.; Staig, S. J.; Weaver, J. D., Facile Synthesis of Z-Alkenes Via Uphill Catalysis. *Journal of the American Chemical Society* **2014,** *136*, 5275-5278.
3. Chen, H. L.; Lee, H. M.; Chen, S. H.; Chao, Y.; Chang, M. B., Review of Plasma Catalysis on Hydrocarbon Reforming for Hydrogen Production—Interaction, Integration, and Prospects. *Applied Catalysis B: Environmental* **2008,** *85*, 1-9.
4. Jin, Z.; Li, Q.; Zheng, X.; Xi, C.; Wang, C.; Zhang, H.; Feng, L.; Wang, H.; Chen, Z.; Jiang, Z., Surface Properties of Pt・Cds and Mechanism of Photocatalytic Dehydrogenation of Aqueous Alcohol. *Journal of Photochemistry and Photobiology A: Chemistry* **1993,** *71*, 85-96.
5. Puga, A. V.; Forneli, A.; García, H.; Corma, A., Production of H2 by Ethanol Photoreforming on Au/Tio2. *Advanced Functional Materials* **2014,** *24*, 241-248.
6. Müller, B. R.; Majoni, S.; Memming, R.; Meissner, D., Particle Size and Surface Chemistry in Photoelectrochemical Reactions at Semiconductor Particles. *The Journal of Physical Chemistry B* **1997,** *101*, 2501-2507.
7. Zhang, Q.; Du, C.; Zhao, Q.; Zhou, C.; Yang, S., Visible Light-Driven the Splitting of Ethanol into Hydrogen and Acetaldehyde Catalyzed by Fibrous Agnps/Cds Hybrids at Room Temperature. *Journal of the Taiwan Institute of Chemical Engineers* **2019,** *102*, 182-189.
8. Xing, C.; Liu, Y.; Zhang, Y.; Wang, X.; Guardia, P.; Yao, L.; Han, X.; Zhang, T.; Arbiol, J.; Soler, L.; Chen, Y.; Sivula, K.; Guijarro, N.; Cabot, A.; Llorca, J., A Direct Z-Scheme for the Photocatalytic Hydrogen Production from a Water Ethanol Mixture on Cotio3/Tio2 Heterostructures. *ACS Applied Materials & Interfaces* **2021,** *13*, 449-457.
9. Lu, H.; Zhao, J.; Li, L.; Gong, L.; Zheng, J.; Zhang, L.; Wang, Z.; Zhang, J.; Zhu, Z., Selective Oxidation of Sacrificial Ethanol over Tio2-Based Photocatalysts During Water Splitting. *Energy & Environmental Science* **2011,** *4*, 3384-3388.
10. Zhang, H.; Zhang, W.; Zhao, M.; Yang, P.; Zhu, Z., A Site-Holding Effect of Tio2 Surface Hydroxyl in the Photocatalytic Direct Synthesis of 1,1-Diethoxyethane from Ethanol. *Chemical Communications* **2017,** *53*, 1518-1521.
11. Yang, P.; Zhao, J.; Cao, B.; Li, L.; Wang, Z.; Tian, X.; Jia, S.; Zhu, Z., Selective Photocatalytic C⍰C Coupling of Bioethanol into 2,3-Butanediol over Pt-Decorated Hydroxyl-Group-Tunable Tio2 Photocatalysts. *ChemCatChem* **2015,** *7*, 2384-2390.
12. Zhang, H.; Xie, S.; Hu, J.; Wu, X.; Zhang, Q.; Cheng, J.; Wang, Y., C–H Activations of Methanol and Ethanol and C–C Couplings into Diols by Zinc–Indium–Sulfide under Visible Light. *Chemical Communications* **2020,** *56*, 1776-1779.
13. Xie, S.; Shen, Z.; Deng, J.; Guo, P.; Zhang, Q.; Zhang, H.; Ma, C.; Jiang, Z.; Cheng, J.; Deng, D.; Wang, Y., Visible Light-Driven C−H Activation and C–C Coupling of Methanol into Ethylene Glycol. *Nature Communications* **2018,** *9*, 1181.
14. Chen, L.; Gu, W.; Zhu, X.; Wang, F.; Song, Y.; Hu, J., Highly Efficient Hydrogen and Ethylene Glycol Photoproduction from Aqueous Methanol Solution by Zns and an in Situ Spin Trapping Investigation. *Journal of Photochemistry and Photobiology A: Chemistry* **1993,** *74*, 85-89.
15. Yanagida, S.; Kawakami, H.; Midori, Y.; Kizumoto, H.; Pac, C.; Wada, Y., Semiconductor Photocatalysis. Zns-Nanocrystallite-Catalyzed Photooxidation of Organic Compounds. *Bulletin of the Chemical Society of Japan* **2006,** *68*, 1811-1823.
16. Savateev, O., Database of Photocatalytic Dehydrogenation Reactions. V1 ed.; Savateev, O., Ed. CUHK Research Data Repository: 2024.
17. Marchi, M.; Melchionna, M.; Fornasiero, P. In *Photocatalytic Hydrogen Production for Sustainable Energy*, 2023; pp 165-190.

18. Qi, M.-Y.; Conte, M.; Anpo, M.; Tang, Z.-R.; Xu, Y.-J., Cooperative Coupling of Oxidative Organic Synthesis and Hydrogen Production over Semiconductor-Based Photocatalysts. *Chemical Reviews* **2021,** *121*, 13051-13085.

19. Huang, C.-Y.; Li, J.; Li, C.-J., A Cross-Dehydrogenative C(Sp3)−H Heteroarylation Via Photo-Induced Catalytic Chlorine Radical Generation. *Nature Communications* **2021,** *12*, 4010.

20. Zhong, J.-J.; Meng, Q.-Y.; Liu, B.; Li, X.-B.; Gao, X.-W.; Lei, T.; Wu, C.-J.; Li, Z.-J.; Tung, C.-H.; Wu, L.-Z., Cross-Coupling Hydrogen Evolution Reaction in Homogeneous Solution without Noble Metals. *Organic Letters* **2014,** *16*, 1988-1991.

21. Cao, H.; Jiang, H.; Feng, H.; Kwan, J. M. C.; Liu, X.; Wu, J., Photo-Induced Decarboxylative Heck-Type Coupling of Unactivated Aliphatic Acids and Terminal Alkenes in the Absence of Sacrificial Hydrogen Acceptors. *Journal of the American Chemical Society* **2018,** *140*, 16360-16367.

22. Lin, J.; Li, Z.; Kan, J.; Huang, S.; Su, W.; Li, Y., Photo-Driven Redox-Neutral Decarboxylative Carbon-Hydrogen Trifluoromethylation of (Hetero)Arenes with Trifluoroacetic Acid. *Nature Communications* **2017,** *8*, 14353.

23. Tian, W.-F.; Hu, C.-H.; He, K.-H.; He, X.-Y.; Li, Y., Visible-Light Photoredox-Catalyzed Decarboxylative Alkylation of Heteroarenes Using Carboxylic Acids with Hydrogen Release. *Organic Letters* **2019,** *21*, 6930-6935.

24. Everson, D. A.; Weix, D. J., Cross-Electrophile Coupling: Principles of Reactivity and Selectivity. *The Journal of Organic Chemistry* **2014,** *79*, 4793-4798.

25. Achilleos, D. S.; Yang, W.; Kasap, H.; Savateev, A.; Markushyna, Y.; Durrant, J. R.; Reisner, E., Solar Reforming of Biomass with Homogeneous Carbon Dots. *Angewandte Chemie International Edition* **2020,** *59*, 18184-18188.

26. Achilleos, D. S.; Kasap, H.; Reisner, E., Photocatalytic Hydrogen Generation Coupled to Pollutant Utilisation Using Carbon Dots Produced from Biomass. *Green Chemistry* **2020,** *22*, 2831-2839.

27. Beckedorf, M.; Holland, J.; Godin, R., Cobalt-Loaded Carbon Nitride Demonstrates Enhanced Photocatalytic Production of H2 from Lignocellulosic Biomass Components. *Artificial Photosynthesis* **2024**.

28. Osterloh, F. E., Photocatalysis Versus Photosynthesis: A Sensitivity Analysis of Devices for Solar Energy Conversion and Chemical Transformations. *ACS Energy Letters* **2017,** *2*, 445-453.

29. U. Dighe, S.; Juliá, F.; Luridiana, A.; Douglas, J. J.; Leonori, D., A Photochemical Dehydrogenative Strategy for Aniline Synthesis. *Nature* **2020,** *584*, 75-81.

30. Frank, B. D.; Antonietti, M.; Giusto, P.; Zeininger, L., Photocharging of Carbon Nitride Thin Films for Controllable Manipulation of Droplet Force Gradient Sensors. *Journal of the American Chemical Society* **2023,** *145*, 24476-24481.

31. Li, Z.-J.; Zhan, F.; Xiao, H.; Zhang, X.; Kong, Q.-Y.; Fan, X.-B.; Liu, W.-Q.; Huang, M.-Y.; Huang, C.; Gao, Y.-J.; Li, X.-B.; Meng, Q.-Y.; Feng, K.; Chen, B.; Tung, C.-H.; Zhao, H.-F.; Tao, Y.; Wu, L.-Z., Tracking Co(I) Intermediate in Operando in Photocatalytic Hydrogen Evolution by X-Ray Transient Absorption Spectroscopy and Dft Calculation. *The Journal of Physical Chemistry Letters* **2016,** *7*, 5253-5258.

32. Smolentsev, G.; Cecconi, B.; Guda, A.; Chavarot-Kerlidou, M.; van Bokhoven, J. A.; Nachtegaal, M.; Artero, V., Microsecond X-Ray Absorption Spectroscopy Identification of Coi Intermediates in Cobaloxime-Catalyzed Hydrogen Evolution. *Chemistry – A European Journal* **2015,** *21*, 15158-15162.

33. Galushchinskiy, A.; Zou, Y.; Odutola, J.; Nikačević, P.; Shi, J.-W.; Tkachenko, N.; López, N.; Farràs, P.; Savateev, O., Insights into the Role of Graphitic Carbon Nitride as a Photobase in Proton-Coupled Electron Transfer in (Sp3)C−H Oxygenation of Oxazolidinones. *Angewandte Chemie International Edition* **2023,** *62*, e202301815.

34. Chai, J.-D.; Head-Gordon, M., Long-Range Corrected Hybrid Density Functionals with Damped Atom–Atom Dispersion Corrections. *Physical Chemistry Chemical Physics* **2008,** *10*, 6615-6620.

35. Marenich, A. V.; Cramer, C. J.; Truhlar, D. G., Universal Solvation Model Based on Solute Electron Density and on a Continuum Model of the Solvent Defined by the Bulk Dielectric Constant and Atomic Surface Tensions. *The Journal of Physical Chemistry B* **2009,** *113*, 6378-6396.

36. McQuarrie, D. A.; Simon, J. D., *Physical Chemistry: A Molecular Approach*. University Science Books: 1997.

37. Lotsch, B. V.; Döblinger, M.; Sehnert, J.; Seyfarth, L.; Senker, J.; Oeckler, O.; Schnick, W., Unmasking Melon by a Complementary Approach Employing Electron Diffraction, Solid-State Nmr Spectroscopy, and Theoretical Calculations—Structural Characterization of a Carbon Nitride Polymer. *Chemistry – A European Journal* **2007,** *13*, 4969-4980.

38. Seyfarth, L.; Seyfarth, J.; Lotsch, B. V.; Schnick, W.; Senker, J., Tackling the Stacking Disorder of Melon—Structure Elucidation in a Semicrystalline Material. *Physical Chemistry Chemical Physics* **2010,** *12*, 2227-2237.

39. Hammer, B.; Hansen, L. B.; Nørskov, J. K., Improved Adsorption Energetics within Density-Functional Theory Using Revised Perdew-Burke-Ernzerhof Functionals. *Physical Review B* **1999,** *59*, 7413-7421.

40. Grimme, S.; Antony, J.; Ehrlich, S.; Krieg, H., A Consistent and Accurate Ab Initio Parametrization of Density Functional Dispersion Correction (Dft-D) for the 94 Elements H-Pu. *The Journal of Chemical Physics* **2010,** *132*.